RESEARCH PAPER

On the use of complex band structure to study valley photovoltaics: toward efficient hot carrier extraction

David K. Ferry ©,**a,*** **Vincent R. Whiteside** ©,**b** and **Ian R. Sellers** **b**
aArizona State University, School of Electrical, Computer, and Energy Engineering, Tempe, Arizona, United States
bUniversity at Buffalo, The State University of New York, Department of Electrical Engineering, Buffalo, New York, United States

ABSTRACT. Hot carrier solar cells were first proposed many decades ago. Over the intervening years, there has been a continuing quest to create these cells, which hold promise to shatter the Shockley–Queisser efficiency limit on single-junction solar cells. One approach considered is to use satellite valleys of the conduction band as metastable states for storing hot electrons until they can be extracted. Experimental efforts, however, have shown the presence of a barrier between the two materials, likely at the heterostructure interface between the absorber and extraction layer. Transfer across the interface is a real-space event rather than a momentum-space process. If the two bands from, and to, which the electron moves are not perfectly aligned, then tunneling must occur. The determination of the evanescent wave numbers that appear in tunneling coefficients are not the simple ones in textbooks but must be found from the full complex band structure of the two materials. Here, the nature of these evanescent states and their role in the tunneling of carriers across typical interfaces is examined using empirical pseudopotential methods.

1 Introduction

The limit to solar-cell efficiency has long been thought to be the Shockley-Queisser limit.[1] Yet, quite some years ago, it was predicted that this limit could be exceeded with hot carrier solar cells (HCSCs),[2] in which photo-excited carriers were induced to retain much of their energy when collected, rather than losing it to phonons in relaxation to the bottom of the conduction (or top of the valence) band. More recently, it was suggested that a hot carrier solar cell could use the satellite valleys of the conduction band as metastable valleys to store the hot carriers and prevent their emission of phonons in relaxation processes,[3] provided that these carriers could be collected from these satellite valleys. This latter work suggested that a suitable cell could be fabricated using heterojunctions of InGaAs and InAlAs.[4] The use of the satellite valleys in this manner has come to be termed *valley photovoltaics*.[5] The idea of such a cell, and the environment in which it would operate, has been reviewed recently.[6]

Subsequently, however, cells fabricated in this manner, while showing the presence of significant hot carriers thought to be in the satellite valleys, exhibited a significant barrier to the

*Address all correspondence to D. K. Ferry, ferry@asu.edu
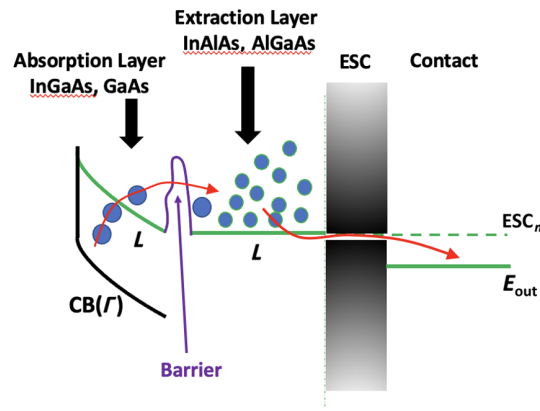
Fig 1 Rendition of a portion of the hot carrier solar cell including the absorption layer, the extraction layer, an energy selective contact, and the actual contact. Experiments on these cells show the presence of a barrier inhibiting carrier extraction,[4] as indicated between the absorption layer and the extraction layer. The absorption layer and extraction layer are both *n*-type.

extraction of these hot carriers.[7] Because extraction of hot carriers (or any carriers) requires real-space transfer from one material to another, it is thought that the barrier involved in the latter work is likely a real-space tunneling barrier that may arise from a mismatch in energy between the two materials in the heterostructure. This is illustrated in Fig. 1, where the absorption layer, extraction layer, energy-selective exit layer, and contact are shown. Not shown is the *p*-layer that would sit to the left of the absorption layer and provide the *p-n* junction. Operation of this type of cell uses the energy of the photo-excited carriers, or the field in the *n*-type layer, to excite carriers into the *L* valleys of this material (either InGaAs or GaAs in this study). These carriers then need to transfer to the (preferably) *L* valleys of the extraction layer, from which they can be collected as a photo-current. Shown between the absorption layer and the extraction is a barrier that experiments have shown likely exists and blocks an effective extraction of the photoelectrons. This barrier creates several problems. First, as mentioned, it blocks the effective transfer of the carriers from the absorption layer to the extraction layer. Second, it prolongs the time the carriers remain in the satellite valleys. If they remain here sufficiently long, they can relax to the Γ valley by the emission of a zone-edge phonon, which dissipates substantial energy to the lattice. Normally, the scattering rate from Γ to *L* is much larger than the reverse process, due to the multiplicity of *L* valleys and the larger mass in the latter valleys (both of which contribute to the larger density of states in the *L* valleys). The scattering rate from Γ to *L* is of the order of $2\text{--}6 \times 10^{13}$ s^{-1} and an order of magnitude less for the reverse process.[3] While the tunneling time through a barrier is a controversial subject,[8] an estimate can be made from the velocity and barrier thickness. This is usually much less than 0.1 ps, comparable to the scattering rates discussed above, but unlikely to be a limiting factor.

Probing the physics of hot carriers in satellite valleys is difficult because most measurements are indirect.[9] In heterostructures, transfer of carriers from one material to the other, across the interface between the two materials is a real-space phenomenon. If the bands in which the carriers are located are not perfectly aligned, then the process must involve "tunneling" across the interface, because the carriers in the higher-lying bands do not have real states available to match those in the lower-lying bands of other materials. This tunneling does not involve the simple models used in introductory quantum mechanic books. Moreover, the simple models found in textbooks are not applicable to heterostructures such as those considered here. In the textbook models with a simple tunnel barrier, one matches the wave function and its derivative at each of the two potential transitions. This is improper for a heterojunction of dissimilar materials. When an electron crosses the interface between two dissimilar materials, this electron has to satisfy current continuity, as required by both Kirchhoff's current law and Maxwell's equations. The current carried by a single electron is just $j = ev$, where e is the charge and v is the velocity of the electron. That is, the matching condition requires that the velocity normal to the interface must be equal on both sides[10]

$$\frac{1}{m_1}\frac{\partial \psi_1}{\partial z} = \frac{1}{m_2}\frac{\partial \psi_2}{\partial z}, \tag{1}$$

where the subscripts 1 and 2 refer to the wave functions in the left-hand and right-hand materials, respectively. Alternatively, this may be expressed as

$$\frac{\hbar k_{z,1}}{m_1} = \frac{\hbar k_{z,2}}{m_2}, \tag{2}$$

where m is the effective mass in the appropriate valleys of either material.

Another problem is that the imaginary wave vector is proportional to the square root of the actual barrier potential and is usually a function of position. In the simple approximation, it has been assumed that the band gap is infinite. Such an approximation is not appropriate for semiconductors, especially those with relatively small band gaps. The real values of tunneling coefficients in condensed matter depend upon the non-propagating, or evanescent, states associated with the regular band structure.

Some indications of tunneling can be obtained by examining the evanescent states of the electrons that arise from the so-called *complex* band structure.[11–14] Normal band structure calculations determine the allowed energy bands for real values of the wave number **k**. However, a more complete picture also determines the energy for evanescent states in which k is imaginary, as in tunneling situations.[15] These evanescent states and their connection to the allowed energy bands provide useful information for studying carrier motion within heterostructures in which tunneling contributes to the transport. Determining the values of k near the interface of interest allows one to estimate the decay constant of the evanescent wave, and this can be used to estimate the tunneling probability through a simple barrier.

The most important region that is commonly studied via the complex band structure is that around the minimum of the conduction band (and the maximum of the valence band). This is because most tunneling structures use carriers that exist in the lowest conduction bands (or highest valence bands), both of which are at the Γ point in the Brillouin zone of the III–V direct gap materials. An important point is that the evanescent states connect various parts of the normal energy bands. For example, the most common branch of the complex band structure connects the minimum of the conduction band and the maximum of the light-hole valence band in a direct-gap semiconductor, as is indicated in $\mathbf{k} \cdot \mathbf{p}$ perturbation theory coupled to the spin-orbit interaction.[11,16] The complex band structure is useful for more than tunneling, as it is critical to surface and interface physics, particularly in heterostructures, and it has recently become of great interest for understanding nanowires formed from III–V materials.[17]

In valley photovoltaic devices, as opposed to normal tunneling or interfaces, interest lies in the higher-lying satellite valleys of the conduction band. In most direct gap III–V materials, the valleys of interest are the L valleys, lying at the zone edge along (111). It is these valleys that have been suggested for hot carrier storage,[3] and it is the complex band structure around these valleys that is of interest.

In this paper, the complex band structure will be examined for the materials InGaAs and InAlAs, as well as for GaAs and AlGaAs, the latter of which have been suggested as alternative materials for valley photovoltaics. The calculations are carried out using local empirical pseudopotentials.[18–20] In particular, the evanescent states that originate from the L valleys of the conduction band will be examined. To the authors' knowledge, this is the first study for evanescent states originating from these (111) satellite valleys of the conduction band.

In the following sections, a brief review of the methods for determining the complex band structure will be given, followed by a discussion for (i) InGaAs and InAlAs and (ii) GaAs and AlGaAs in Sec. 3. Finally, a discussion of the impact of these on the understanding in valley photovoltaics will be presented in Sec. 4.

2 Complex Band Structure

The empirical pseudopotential method (EPM) computes the energy bands in momentum space but matches the calculated bands to available experimental data for the positions of various critical points. In EPM, the pseudopotential is Fourier transformed in terms of reciprocal lattice vectors as[15]

$$V_P(\boldsymbol{r} - \boldsymbol{r}_0) = \sum_{\boldsymbol{G}} \tilde{V}_1(\boldsymbol{G})e^{i\boldsymbol{G}\cdot(\boldsymbol{r}-\boldsymbol{r}_0)} , \tag{3}$$

where $\boldsymbol{r}_0$ is the atomic position of the atom of interest and $\boldsymbol{G}$ is a reciprocal lattice vector. In practice, only a limited number of such vectors are used for the Fourier transform due to computational difficulties (to be discussed below). The actual Fourier transform of the pseudopotential is given as

$$\tilde{V}_1(\boldsymbol{G}) = \frac{1}{\Omega} \int d^3r\, e^{-i\boldsymbol{G}\cdot\boldsymbol{r}} V_P(\boldsymbol{r}), \tag{4}$$

where the atomic position is assumed in the integral. The quantity Ω is the volume of the unit cell. In these materials, there are two atoms per unit cell, and these produce two pseudopotentials, which are normally combined and then separated into symmetric and anti-symmetry components, with the coordinate origin taken between the two atoms. This leads to an equation for the energy bands as[21]

$$\sum_{\boldsymbol{G}} C_{\boldsymbol{G}}\{[\frac{\hbar^2}{2m_0}(\boldsymbol{k}+\boldsymbol{G})^2 - E]\delta_{\boldsymbol{G},\boldsymbol{G}'} + [\boldsymbol{k}+\boldsymbol{G}'|V_c(\boldsymbol{r})|\boldsymbol{k}+\boldsymbol{G}]\} = 0. \tag{5}$$

There is an equation like this for each value of $\boldsymbol{G}'$. The last term in Eq. (5) is the Fourier transform of the pseudopotential terms, both even and odd, but the important point is that this Fourier transform becomes

$$V_c(\boldsymbol{G} - \boldsymbol{G}'). \tag{6}$$

That is, it is a function only of the difference between the two reciprocal lattice vectors.[20] This latter term is a scalar and thus depends only upon the magnitude of the difference between the two vectors. The different terms that arise are Fourier coefficients of the pseudopotential in this representation. These coefficients fall off fairly rapidly as the magnitude of the difference increases so that only a small number is required to represent the energy bands. For example, consider two vectors $(2,2,0)$ and $(2,\bar{2},2)$ (the overbar represents a negative direction) would have the difference $(0,4,\bar{2})$ or a magnitude of 20. By this magnitude, the Fourier coefficient is essentially unimportant in the calculation. The term $V_c(0)$ gives a uniform shift of the bands and is usually used to set the energy of the top of the valence band to 0 and of the order of seven to eight Fourier components that are usually adequate to describe the energy bands.

In general, nonlocal corrections to the pseudopotential are added to account for angular variations around the atom that may arise,[20,22] and these are added in the present study, although they make only small corrections in EPM, which is adjusted to fit the experiment (hence *empirical*). As mentioned above, usually only a limited number of reciprocal lattice vectors are used because the number determines the size of the matrix to be inverted.

In the present calculation, 137 plane waves (values of $\boldsymbol{G}$) are used, which leads to reciprocal lattice difference vectors in Eq. (6) up to $(4,2,2)$, which accounts for a magnitude $|\boldsymbol{G} - \boldsymbol{G}'|^2 = 24$, with the vectors in units of $2\pi/a$,[23] and results, for example, from the magnitude of the vector that spans the two vectors of this last set $(4, 2, 2)$ and $(\bar{4}, \bar{2}, \bar{2})$. This considers reciprocal lattice vectors up to the ninth nearest neighbor and gives a cutoff of $\sim$100 eV, which has proven adequate for EPM in these materials in the past.[20] This also is much less than needed for a first-principle approach to a density-functional calculation. The general band structure for $In_{0.53}Ga_{0.47}As$ as calculated by this technique is presented in Fig. 2.

Normally, one solves Eq. (5) by taking a large number of values of $\mathbf{k}$ for various directions and points in the Brillouin zone and finding the corresponding energy. One may note that once the Fourier transform of the pseudopotential is used, the momentum wave vector $\mathbf{k}$ appears only in the first term of Eq. (5). One problem with the complex band structure is that it can have a large variation in energy for a small variation in k. Indeed, there are critical areas where the derivative of the energy curves is infinite. Consequently, it is more stable when computing the complex band structure to take values of energy and find the corresponding values of wave number.

This is most easily set by expanding the Hamiltonian (plus energy, the first term in Eq. (5)) in the form[21]
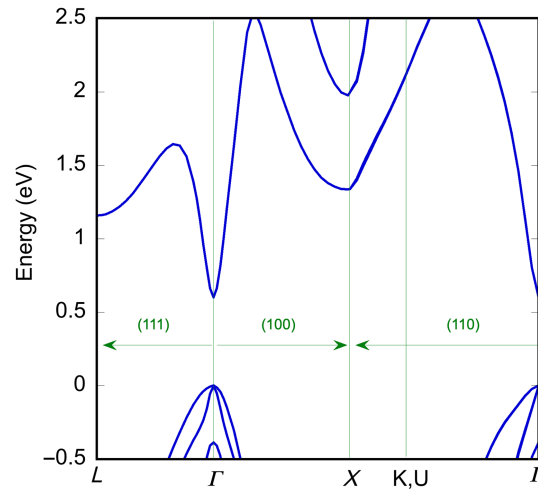
Fig. 2 Real band structure of In$_{0.53}$Ga$_{0.47}$As computed with a non-local EPM. Only the regions around the principal energy gap are shown. This band structure is computed along three principal crystal directions which are indicated in the figure. For the (110), the X point lies in the second zone.

$$H(\mathbf{k}) = H^0(\mathbf{k}_0) + H^1(\mathbf{k}_0)k_z + k_z^2, \tag{7}$$

where $\mathbf{k}_0$ is the lattice point around which the evanescent states are to be determined and k_z is the difference wave number for which the imaginary states are desired (assumed to be the direction normal to the heterostructure interface). Then, the Hamiltonian Eq. (3) can be transformed into an eigenvalue equation for k_z as[21]

$$\begin{bmatrix} 0 & 1 \\ H^0(\mathbf{k}_0) & H^1(\mathbf{k}_0) \end{bmatrix} \begin{bmatrix} C \\ C_1 \end{bmatrix} = k_z \begin{bmatrix} C \\ C_1 \end{bmatrix}, \tag{8}$$

where $C_1 = k_z C$ and C represents a column vector of the coefficients C_G in Eq. (5). As a result, the imaginary band structure is now a simple eigenvalue equation that may be evaluated at given values for the energy and the wave number $\mathbf{k}_0$.

As mentioned, the complex band structure around the L valley minimum, located at the zone edge along (111) is of interest. This complex structure is shown in Fig. 3. The red curves are lines that originate exactly at one of the real bands at L, while the blue lines are shifted by a (400) reciprocal lattice vector, although these will exist in the first zone once the full periodicity of the
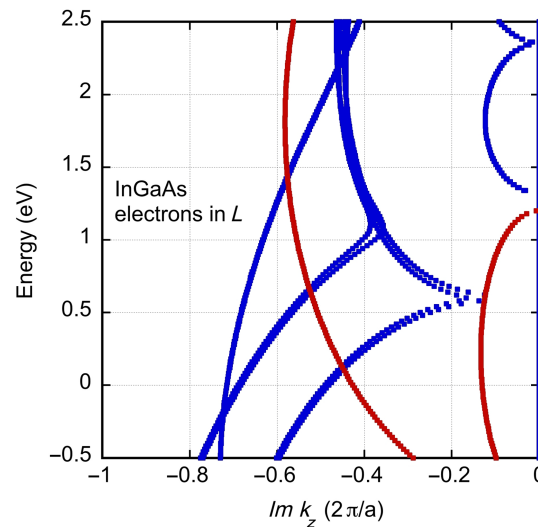
Fig. 3 Complex bands for k along (001) measured away from the L valley minimum at (111), at the right-hand side. The difference in the colors is discussed in the text.

lattice is invoked. Nevertheless, only the red curves will be considered in the following discussion of possible heterostructures for use in valley photovoltaic devices.

3 InGaAs and InAlAs

As discussed in the introduction, the original concept of valley photovoltaics considered a heterojunction structure using $In_{0.53}Ga_{0.47}As$ and $In_{0.52}Al_{0.48}As$.[3] These two materials are both lattice-matched to an InP substrate and can be grown by standard approaches using either molecular-beam epitaxy or metal-organic vapor-phase epitaxy. Here, a heavily doped InAlAs p-layer followed by a lightly doped InGaAs n-layer forms the p-n junction. This was followed by an additional n-doped InAlAs layer through which the hot carriers were to be extracted, as shown in Fig. 1.

The idea was that the large band offset between the conduction band of InGaAs and the conduction band of InAlAs would effectively block extraction from the carriers that relaxed to the Γ band minimum, effectively allowing only the hot carriers in the L valleys to transit to this top heterointerface layer. The InGaAs material has a smaller band gap of about ~0.75 eV,[24] and the position of the L minimum lies about ~0.5 eV above the conduction band minimum. Moreover, the direct energy gap in InGaAs lies at the peak of the Shockley–Queisser efficiency response.[1]

The InAlAs, on the other hand, has a direct energy gap of 1.565 eV, with the minimum of the conduction band lying some 0.53 eV above that of InGaAs.[25] The alignment of the various bands is shown in Fig. 4 for the two n-type materials of this heterostructure (no correction for doping is shown).

The first problem with the initially proposed structure (and those built and tested[7]) is the fact that the L valleys of InAlAs (and other heterointerface barriers) lie some 255 meV above those of the InGaAs. This presents a significant barrier to direct transfer across the heterostructure interface from one material to the other. This, by itself, could explain the observed barrier to current extraction in the actual structure. On the other hand, the Γ valley of the InAlAs barrier lies (in this example) ~80 meV above the L minima of the InGaAs absorber. Electrons in the latter could transfer to the Γ valley of the InAlAs by absorption of an L point phonon of sufficient energy. Unfortunately, the highest energy phonon in the InAlAs is ~46 meV,[26] and this is the AlAs-derived LO_2 mode at the zone center. Hence, even the relaxed electrons in the InGaAs L valleys cannot make it to the InAlAs Γ valley. This however does not address the question of whether these latter electrons can tunnel to the InAlAs L valleys. To study this, we turn to the complex band structure.

In Fig. 5, the main energy bands of InGaAs are shown along with the principal bands for the imaginary wave number. It may be seen here that the most important imaginary band (those with the smallest value of complex k) moves downward from the L valleys, as expected from Fig. 3.
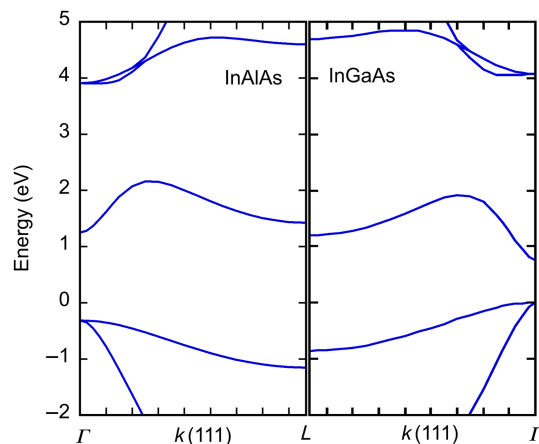
Fig. 4 Band alignment of $In_{0.52}Al_{0.48}As$ and $In_{0.53}Ga_{0.47}As$ are depicted, taking into account the known offset between the conduction band minima of the two materials.
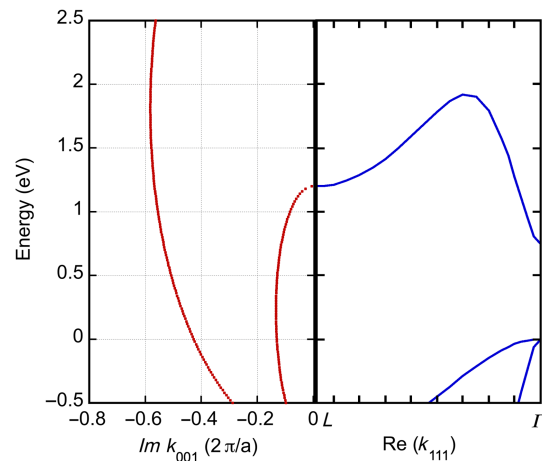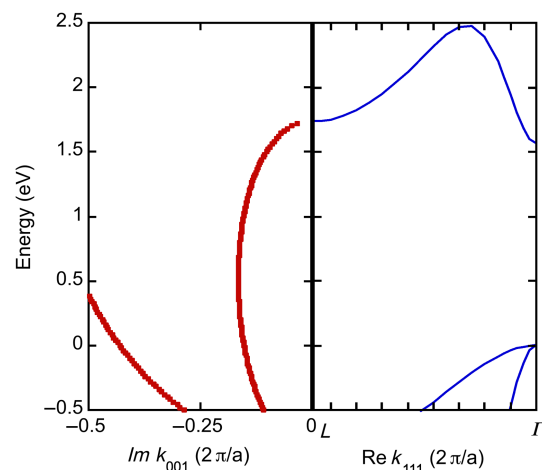
Fig. 5 Principal energy bands for $In_{0.53}Ga_{0.47}As$ (right) and the principal complex bands extending from the L valleys. The left-most of the latter actually arises from a higher-lying L valley.

Thus, it is difficult to see how these bands can support an evanescent wave tunneling across the heterostructure interface.

The important aspect is the value of the imaginary k and the actual physical thickness of the interface of the heterostructure. This must be coupled to the existence of available real energy states on the other side of this interface or the ability to couple to an evanescent wave on the other side of the interface. Nevertheless, the barriers discussed in the previous paragraph make it hard to imagine an effective tunneling with this material structure.

To confirm the above suggestions, the evanescent states in the InAlAs must be considered. In Fig. 6, the main energy bands of this material and the relevant evanescent bands for the L valleys are shown. These have the same general shape as those of the InGaAs. An important point is that the value of the imaginary k is large in this material, primarily because the transition to the InGaAs lies further from the band edge. At the L valley energy of the InGaAs, the imaginary value of k is $\sim 10^7 cm^{-1}$. If the heterostructure were atomically abrupt, then one might expect the tunneling coefficient to be of the order of ~ 0.25, which is not all that small for tunneling. However, if the interface disorder makes the transition region through which tunneling must occur on the order of even 1 nm, then the tunneling coefficient would drop to $\sim 4 \times 10^{-6}$, which would be sufficiently small to block almost all of the current. This appears to be the case in the experiments.[7] Unfortunately, disorder is expected as it is common for growth on top of Al-containing compounds, which is the case in this structure.

Fig. 6 Principal energy bands for $In_{0.52}Al_{0.48}As$ (right) and the principal complex bands extending from the L valleys. The left-most of the latter actually arises from a higher-lying L valley.

4 GaAs and AlGaAs

Heterostructures between AlGaAs and GaAs have long been the preferred approach for III–V-based devices, particularly transistors. Not the least of the reasons for this is that AlAs and GaAs are lattice matched with one another, and this relationship holds across the alloy. Due to this, these materials can be grown with almost atomically precise interfaces,[27] if the AlAs-containing compound is grown on top of the pure GaAs substrate (growth on top of an Al-containing compound is more often complicated due to oxidation of the Al).[28]

Despite extensive studies to try to overcome the problems of the heterostructure of the previous section,[29,30] it is clear that a different materials system from those currently explored above will be required, and the physics more carefully considered. Initial studies indicate that the GaAs-AlGaAs system has promise to overcome the problems outlined earlier. In this section, the advantageous position of this heterostructure will be discussed.

Of course, GaAs-based solar cells are not new, but actually provided the record single-junction efficiency of any thin film solar cell,[31] reaching 27.6% efficiency, or a multi-junction heterostructure,[32] reaching 38.85% efficiency without concentration. In most cases, the GaAs is coupled with other III–V materials or Si in a heterostructure format, and occasionally, this also includes AlGaAs. However, the use of the GaAs/AlGaAs heterostructure here is examined for hot carrier solar cells, which involve using the satellite valleys of both materials for extraction of the hot carriers.

There are some limits for the use of AlGaAs, as it has a direct band gap only for an AlAs composition less than 0.55.[23] Even below this limit, it is generally considered necessary to keep the AlAs composition below ~0.28 to 0.3 to avoid a difficult defect emerging from the conduction band for compositions above this.[33] While this defect, known as the DX center, can occur over a range of compositions extending to as low as 0.22, it is generally felt to be degenerate with the conduction for compositions below those mentioned above.[34] Using these lower compositions is reasonable, because they also allow the L valleys in both AlGaAs and GaAs to lie quite near each other in energy. This may be seen in Fig. 7 for a heterostructure using $Al_{0.25}Ga_{0.75}As$ and in Fig. 8 for a heterostructure using $Al_{0.16}Ga_{0.16}As$.

Studies of the GaAs-AlGaAs heterostructure have shown that the bands align with ~63% of the band gap difference in the conduction bands.[35] This has been used to align the two band structures to one another in these latter figures. For the 25% alloy (Fig. 7), this results in a Γ valley discontinuity of ~230 meV, which should be adequate to prevent electrons in this valley of GaAs from being collected. The discontinuity in the L valleys is ~74 meV, which is an improvement over the previous InAlAs/InGaAs structure but may still be too large to allow effective collection of hot carriers.

With the lower percentage of AlAs (16%, Fig. 8), these numbers become ~210 meV for the Γ valley and ~35 meV for the L valley. The Γ offset should still be large enough to block most electrons from this valley from being collected, and the L valley offset should be low enough to
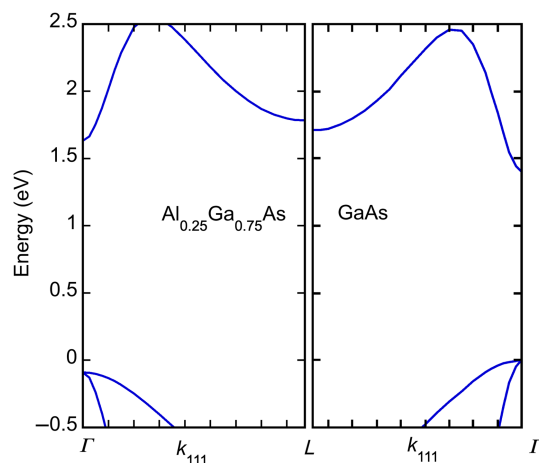
Fig. 7 Alignment of the L and Γ valleys of the conduction is shown for $Al_{0.25}Ga_{0.75}As$ and GaAs. The bands of the former have been shifted by the known band offsets for this heterostructure.
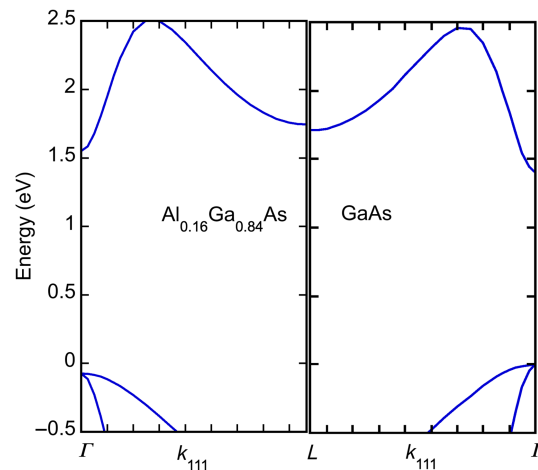
Fig. 8 Alignment of the L and Γ valleys of the conduction is shown for $Al_{0.16}Ga_{0.84}As$ and GaAs. The bands of the former have been shifted by the known band offsets for this heterostructure.

allow efficient collection from the L valleys. This will be examined below with the complex band structure for these heterostructures.

In Fig. 9, the band structure of GaAs, along the (111) direction, is shown along with the complex band structure away from the L point along (001). The imaginary wave number curve extends downward from the L point, just as in the other materials studied, so that this cannot couple to the AlGaAs on its own. However, it will be possible for the comparable branch from the L valley in the AlGaAs to hybridize with this branch, and this should occur quite near the L valley where the wave number curve is fairly flat. Such a hybridization should flatten out the overall curve with an evanescent action smaller than normally expected from the complex band structure of either material. So, the following discussion may be considered to correspond to perhaps a worst-case behavior.

Consider the situation with $Al_{0.25}Ga_{0.75}As$ shown in Fig. 10. The evanescent wave number curves are very similar to those of GaAs, although they of course begin and end at different energies and these are at the L valleys in the AlGaAs. Certainly, the evanescent branch in Fig. 10 passes down through the energy of the L valleys in GaAs, so that there again will be some coupling here, as mentioned above. It was noted earlier that the two sets of L valleys are actually separated by 74 meV in the heterostructure of this composition of AlGaAs and GaAs. At this energy below the L valleys of the AlGaAs, the value of wave number in the main branch is 6×10^6 cm^{-1}. Moreover, if we take a reasonably abrupt interface, the tunneling coefficient is
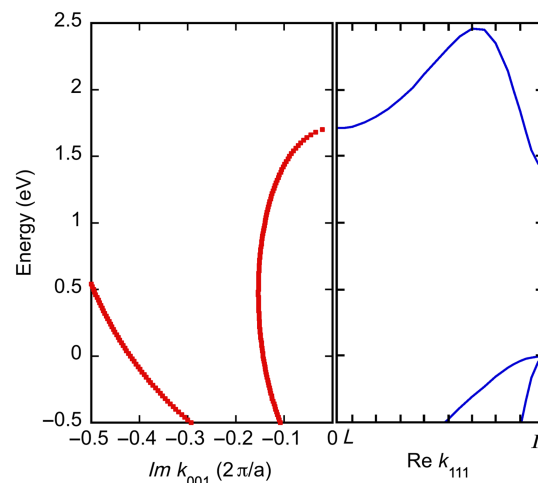
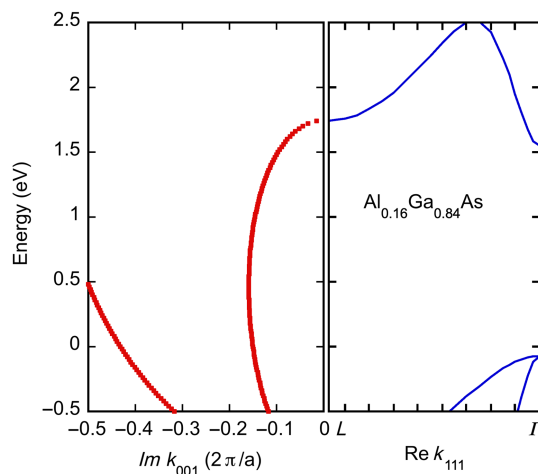**Fig. 9** Real band structure of GaAs along (111) (right) and the complex band structure along (001) extending from the L valleys.
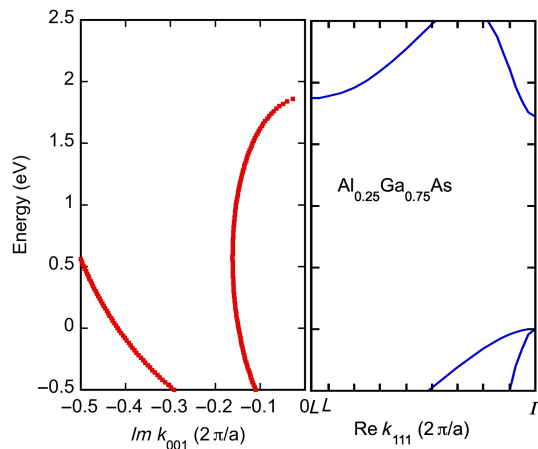
Fig. 10 Real band structure of $Al_{0.25}Ga_{0.75}As$ along (111) (right) and the complex band structure along (001) extending from the L valleys.

likely to be ∼0.5, which is not so large as to cause a significant decay of the wave function, although it still remains a barrier. We will discuss this further in the next section.

Now, turn to the situation with $Al_{0.16}Ga_{0.84}As$ shown in Fig. 11. The evanescent wave number curves are once again very similar to those of GaAs, although they of course begin and end at different energies, although these are at the L valleys in the $Al_{0.16}Ga_{0.84}As$. Certainly, the evanescent branch in Fig. 11 passes down through the energy of the L valleys in GaAs, just as in the previous case, so there will be some coupling here, as mentioned above. In this case, however, the two sets of L valleys are actually separated by only 35 meV (which is only slightly larger than k_BT and is thus likely to be easily overcome with the thermal broadening of the states) in the heterostructure of this composition of AlGaAs and GaAs. This thermal broadening implies that a range of energies are coupled due to the thermal motion of the carriers, and this gives some uncertainty about the band alignments. However, this thermal energy might also give a boost to the electrons, corresponding to a thermal excitation over the barriers, or more likely a thermally assisted tunneling process. This makes the following estimate a lower limit on the likely tunneling. At the above energy below the L valleys of the AlGaAs, the value of wave number is 1.2×10^6 cm^{-1}. If a reasonably abrupt interface is assumed, the tunneling coefficient is likely to be ∼0.88, which suggests a significant tunneling probability in this structure, and it therefore is quite likely that electrons in the L valleys of the GaAs will move easily across the L–L heterointerface into the AlGaAs collector layer. We will discuss this further in the next section.

Fig. 11 Real band structure of $Al_{0.16}Ga_{0.84}As$ along (111) (right) and the complex band structure along (001) extending from the L valleys.

5 Discussion and Conclusion

As discussed in the introduction, advances in valley photovoltaics have yet to realize clear evidence of a hot carrier solar cell based upon this protocol. This has been attributed to the inability to extract hot carriers from the absorption layer. The existence of an L–L barrier in the InAlAs/InGaAs heterointerface has been shown here through the study of the evanescent parts of the band structure of these two materials. This has shown that there is an exponentially small tunneling coefficient that arises from the mismatch in the bands between these two materials that is heightened by the possible lack of atomically abrupt interfaces. Even an interface roughness of just a few atoms in thickness is exceedingly detrimental to the tunneling of carriers from one material to the other, especially with the relatively large values of the evanescent wave number for satellite valley coupling. These results support the observation of poor behavior in experimental studies of devices based upon this material system.[7]

The situation is found to be improved in the AlGaAs/GaAs material system, both by the much better alignment of the L valleys, as well as by the known ability to grow this system with atomic abruptness when AlGaAs is grown on top of GaAs. Here, it is found that the tunneling coefficient for L–L transfer between the two materials could be as large as 0.5 for the use of $Al_{0.25}Ga_{0.75}As$, or as large as 0.88 for the use of $Al_{0.16}Ga_{0.84}As$, in the collector layer. While these numbers may appear to be overly optimistic, there is actually evidence that supports this optimism for valley photovoltaics.[36] However, it must be said that any barrier between the absorption layer and the extraction layer will affect the performance of the cell and must be made as small as possible. Not only does such a barrier hinder the transfer of the carriers, but it also leads to unwanted decay of the L valley population through the emission of zone edge phonons and relaxation to the Γ valley where extraction is essentially forbidden by the band alignments.

In AlGaAs/GaAs high-electron mobility transistors, the expected norm is for all electrons in the AlGaAs to move into the inversion layer in GaAs in cases such as modulation doping.[37] However, hot carriers in the GaAs channel can reach sufficient energy to transfer back into the AlGaAs, through the process known as real-space transfer.[38,39] In later studies, it was found that hot carriers in the GaAs can transfer to the L valleys, from which they readily transfer into the AlGaAs L valleys.[37] In these transistors, this is detrimental to their operation, as free charge in the AlGaAs works to lower the effectiveness of gate action. So, this real-space transfer is unwanted in such devices. However, in valley photovoltaics, this real-space transfer from GaAs to AlGAs is the desired mode of operation for valley photovoltaics. Hence, the above suggestions for the efficacy of this transfer support the use of the AlGaAs/GaAs material system for improved valley photovoltaic devices and perhaps finally achieved hot carrier solar cells.

Code and Data Availability

The data resides with the lead author and can be shared upon receiving a reasonable request.

References

1. W. Shockley and H. J. Queisser, "Detailed balance limit of efficiency of p-n junction solar cells," *J. Appl. Phys.* **32**, 510 (1961).
2. R. T. Ross and A. J. Nozik, "Efficiency of hot-carrier solar energy converters," *J. Appl. Phys.* **53**, 3813 (1982).
3. D. K. Ferry, "In search of a true hot carrier solar cell," *Semicond. Sci. Technol.* **34**, 044001 (2019).
4. H. Esmaielpour et al., "Exploiting intervalley scattering to harness hot carriers in III–V solar cells," *Nature Energy* **5**, 336 (2020).
5. D. K. Ferry et al., "Valley photovoltaics and the search for the hot carrier solar cell," *Proc. Photovolt. Spec. Conf.* **20**, 0498 (2020).
6. D. K. Ferry, V. R. Whiteside, and I. R. Sellers, "Pathways to hot carrier solar cells," *J. Photonics Energy* **12**, 022204 (2022).

7. V. R. Whiteside et al., "The role of intervalley phonons in hot carrier transfer and extraction in type-II InAs/AlAsSb quantum-well solar cells," *Semicond. Sci. Technol.* **34**, 094001 (2019).

8. E. H. Hauge and J. A. Støvneng, "Tunneling times: a critical review," *Rev. Mod. Phys.* **61**, 917 (1989).

9. D. K. Ferry, *Hot carriers in semiconductors*, IOP Publishing, Bristo (2021).

10. G. Bastard, "Superlattice band structure in the envelope-function approximation," *Phys. Rev. B* **24**, 5693 (1981).

11. I. Alstrup, "Surface bands of silicon (111) slabs by a LCAO method," *Surf. Sci.* **20** 335 (1970).

12. D. Z.-Y. Ting, "Multiband and multidimensional quantum transport," *Microelectron. J.* **30**, 985 (1999).

13. A. Jensen et al., "Complex band structure and electronic transmission eigenchannels," *J. Chem. Phys.* **147**, 224104 (2017).

14. M. G. Reuter, "A unified perspective of complex band structure: interpretations, formulations, and applications," *J. Phys.: Cond. Matter* **29**, 053001 (2017).

15. D. K. Ferry, X. Oriols, and J. Weinbub, *Quantum transport in semiconductor devices: simulation using particles*, IOP Publishing, Bristol (2023).

16. E. O. Kane, "Band structure of indium antimonide," *J. Phys. Chem. Sol.* **1**, 249 (1957).

17. J. Okada, F. Hashimoto, and N. Mori, "Equivalent model for band-to-band tunneling simulation of direct gap III–V semiconductor nanowires," *Jpn. J. Appl. Phys.* **60**, 091002 (2021).

18. D. Brust, J. C. Phillips, and F. Bassani, "Critical points and ultraviolet reflectivity of semiconductors," *Phys. Rev. Lett.* **9**, 94 (1962).

19. M. L. Cohen and J. C. Phillips, "Spectral analysis of photoemissive yields in Si, Ge, GaAs, GaSb, InAs, and InSb," *Phys. Rev.* **139**, A912 (1965).

20. J. R. Chelikowsky and M. L. Cohen, "Nonlocal pseudopotential calculations for the electronics structure of eleven diamond and zinc-blende semiconductors," *Phys. Rev. B* **15**, 556 (1976).

21. Y.-C. Chang and J. N. Shulman, "Complex band structures of crystalline solids: an eigenvalue method," *Phys. Rev. B* **25**, 3975 (1982)

22. K. C. Pandey and J. C. Phillips, "Nonlocal pseudopotentials for Ge and GaAs," *Phys. Rev. B* **9**, 1552 1974

23. D. K. Ferry, *Semiconductor bonds and bands*, 2nd ed., IOP Publishing, Bristol (2020).

24. S. Adachi, *Physical properties of III–V semiconductor compounds*, Wiley, New York (1992).

25. M. S. Hybertson, "Band offset transitivity at the InGaAs/InAlAs/InP heterointerfaces," *Appl. Phys. Lett.* **58**, 1759 (1991).

26. A. Milekhin et al., "Optical phonons in InAlAs thin layers: Raman and IR study," *AIP Conf. Proc.* **1199**, 43 (2010).

27. Y. Suzuki, M. Seki, and H. Okamoto, "TEM observation of lattice image of $Ga_xAl_{1-x}As$-AlAs superlattice with high contrast," in *16th Cong. Sol. State Dev. Mat., Kobe, Bus. Cntr. Acad. Phys. Soc. Jpn.*, Tokyo, p. 607 (1984).

28. D. K. Ferry, "Evolution of physics and chemistry of surfaces and interfaces: a perspective of the last 40 years," *J. Vac. Sci. Technol. B* **31**, 048501 (2013).

29. K. R. Dorman et al., "Toward hot carrier extraction in intervalley photovoltaic devices," *ACS Appl. Energy Mat.* **5**, 11159 (2022)

30. K. R. Dorman et al., "Electric field and its effect on hot carriers in InGaAs photovoltaic devices," *IEEE J. Photovolt.* **12**, 1175 (2022).

31. B. M. Kayes et al., "27.6% conversion efficiency, a new record for single-junction solar cells under 1 sun illumination," in *IEEE Photovolt. Spec. Conf.*, IEEE Press, New York, (2011).

32. M. A. Green et al., "Solar cell efficiency tables (version 61)," *Prog. Photovolt.: Res. Appl.* **31**, 3 (2023).

33. D. V. Lang and R. A. Logan, "Large-lattice-relaxation model for persistent photoconductivity in compound semiconductors," *Phys. Rev. Lett.* **39**, 635 (1977).

34. D. V. Lang, R. A. Logan, and M. Jaros, "Trapping characteristics and a donor-complex (DX) model for the persistent-photoconductivity trapping center in Te-doped $Al_xGa_{1-x}As$," *Phys. Rev. B* **19**, 1015 (1979).

35. M. Heiblum, M. I. Nathan, and M. Eizenberg, "Energy band discontinuities measured by internal photoemission," *Appl. Phys. Lett.* **47**, 503 (1985).

36. U. Ravaioli and D. K. Ferry, "MODFET ensemble Monte Carlo model including the quasi-two-dimensional electron gas," *IEEE Trans. Electron Devices* **33**, 677 (1986).

37. R. Dingle et al., "Electron mobilities in modulation-doped semiconductor heterojunction superlattices," *Appl. Phys. Lett.* **33**, 665 (1978).

38. K. Hess, "Real-space transfer: generalized approach to transport in confined geometries," *Sol. State Electron.* **31**, 319 (1988).

39. I. C. Kizilyalli and K. Hess, "Physics of real-space transfer transistors," *J. Appl. Phys.* **65**, 2005 (1989).

David K. Ferry is Regents' Professor Emeritus at Arizona State University. He came to ASU in 1983 following stints at Texas Tech University, the Office of Naval Research, and Colorado State University. His research is focused on semiconductors, as well as quantum effects in devices and

materials. He received the 1999 Cledo Brunetti Award from IEEE and is a Fellow of this group as well as the APS and the IOP.

Vincent R. Whiteside is currently a research scientist in the Electrical Engineering Department at the University at Buffalo SUNY. Our research is focused on novel materials and devices for next generation photovoltaics with an emphasis on developing a 'hot' carrier solar cell. Other research focuses on thin film technologies: mainly perovskite and CIGS solar cells, with regards to fundamental properties and the underlying limiting factors pertaining to the commercial viability for terrestrial, and space applications.

Ian R. Sellers is a professor in the Department of Electrical Engineering and adjunct professor in the Department of Physics at the University at Buffalo SUNY. Professor Sellers' research is focused on the development and investigation of novel materials and devices for next generation photovoltaics. Specific programs involve hot carrier dynamics in III–V and perovskite systems, defect formation and stability of thin-film CIGS and perovskite solar cells, as well as their suitability for deep space power applications.